CrossMark

RESEARCH ARTICLE

The opening subplinian phase of the Hekla 1991 eruption: properties of the tephra fall deposit

Jonas Gudnason[1,3] · Thor Thordarson[1] · Bruce F. Houghton[2] · Gudrun Larsen[3]

Abstract The 1991 Hekla eruption started on 17th of January with an intense 50-min-long explosive phase that transitioned into fire fountain activity lasting for 2 days. The eruptive plume rose to maximum height in about 10 min and the total mass of tephra deposited from the opening phase was 8.6×10^9 kg (VEI 3 event). The principal axis of tephra fall is to the NNE of Hekla and grain-size analysis reveals a systematic decrease in grain-size away from source. Majority of sample sites show typically unimodal grain-size distributions, although a few have bimodal distributions where the secondary mode is a subtle finer peak. The calculated total grain-size distribution (TGSD) is bimodal, with a coarse primary peak (-3.5 to -2.5 φ) and a subordinate fine peak (2.5 to 3.5 φ). The coarse peak is lapilli-dominated and was deposited within the first 25 km of transport, whereas the fine peak is coarse-ash-dominated and fits well with the modal grain-size of samples deposited >65 km from Hekla. Ascent rate of the magma and conditions for vesiculation in the shallow conduit became increasingly uniform with time through the 1991 opening phase.

✉ Jonas Gudnason
jog4@hi.is

1 Faculty of Earth Sciences, University of Iceland, Reykjavík, Iceland

2 Department of Geology and Geophysics, University of Hawaii, Honolulu, HI, USA

3 Institute of Earth Sciences, University of Iceland, Reykjavík, Iceland

Introduction

Tephra fall deposits (i.e. pyroclasts deposited by fallout from an eruption plume) of volcanic eruptions contain invaluable information that can be used for assessing eruption parameters such as magnitude, intensity, and eruption plume heights (e.g. Walker 1973; Newhall and Self 1982; Carey and Sparks 1986; Pyle 1989; Bonadonna et al. 1998; Mastin et al. 2009). Selected dispersal parameters (e.g. thinning rate and half distances for clast size) are used to determine eruptive volume and intensity (Pyle 1989; Fierstein and Nathenson 1992; Bonadonna and Houghton 2005; Bonadonna and Costa 2012), while mechanisms of magma fragmentation and eruption dynamics are inferred from the study of the ejected pyroclasts (i.e. tephra clasts) (e.g. Kaminski and Jaupart 1998; Kueppers et al. 2006; Carey et al. 2009; Eychenne et al. 2011) and of total grain-size distribution (TGSD), which is also a critical parameter for numerical models of tephra transport and sedimentation (e.g. Carey and Sigurdsson 1982; Bonadonna and Houghton 2005; Durant et al. 2009; Eychenne et al. 2015). These parameters along with quantification of rates of magma ascent, degassing, and crystallization in the shallow conduit from studies of microtextures provide the best constraints on eruption dynamics (e.g. Houghton and Wilson 1989; Klug and Cashman 1996; Gurioli et al. 2005; Lautze and Houghton 2006; Polacci et al. 2006).

Hekla is one of the most active volcanic systems in Iceland, with at least 23 events in the last 900 years, 18 of which took place at the Hekla central volcano (Thordarson and Larsen 2007). Hekla eruptions start highly explosively (subplinian to Plinian intensity; Janebo et al. 2016; this study), and

Springer

typically with little warning, only tens of minutes (e.g. Thorarinsson 1968; Grönvold et al. 1983; Gudmundsson et al. 1992; Soosalu et al. 2003; Thordarson and Larsen 2007). The drivers for the high intensity of the opening phase are largely unexplored. The fact that the eruptions began with very little warning further emphasizes the importance of better understanding of the explosive opening phases of Hekla events.

The 1991 eruption is ideal for addressing the intricacies of Hekla's opening explosive phases, because its chronology and tephra fall are exceptionally well documented (Gudmundsson et al. 1992; Larsen et al. 1992). In this paper we investigate the 1991 opening phase in order to better quantify the dynamics of the explosive activity as well as the associated eruption source parameters. This is achieved by (1) reassessment of dispersal and volume of the 1991 tephra; (2) comparison of the measured plume height to conventional empirical estimates of plume height from field data; (3) grain-size analyses of strategically selected samples and determined TGSD; (4) density of pumice clasts; and (5) fining in grain-size with distance from source used to constrain rates of tephra sedimentation.

Hekla

Hekla central volcano (63.98°N, 19.70°W; 1490 m a.s.l.) sits within a SW-NE trending fissure swarm that is ~40 km long and ~19 km wide (Fig. 1; e.g. Jakobsson 1979; Jóhannesson and Sæmundsson 1998). Its NW to SE profile has the conical form that typifies stratovolcanoes, while its SW to NE profile is more elongate (Fig. 1c, d). The elongation reflects a ~5-km-long linear vent system that becomes partly or fully active during most eruptions (e.g. Thorarinsson 1968; Thorarinsson and Sigvaldason 1972; Grönvold et al. 1983; Gudmundsson et al. 1992; Larsen et al. 1992; Höskuldsson et al. 2007).

Hekla post glacial eruptive activity has been of three types: (I) effusive fissure eruptions, primarily basaltic; (II) Plinian eruptions of ~70 wt% SiO_2 magma; and (III) hybrid subplinan-Plinian explosive to effusive eruptions. Effusive fissure eruptions (type I) take place on the Hekla fissure swarm outside the Hekla central volcano. The most recent example is the 1913 Lambafit eruption to the NE of Hekla. Lava flows older than 4300 years and younger than 1500 years erupted SW and NE of Hekla, whereas between 4300 and 2000 years ago activity peaked SE and S of Hekla at Vatnafjöll (Jóhannesson and Einarsson 1990). Examples of Plinian eruptions (type II) are the silicic H1, H3, H4, and H5 tephra layers. These large eruptions produced tephra layers that cover up to 80% of Iceland and have volumes up to 13 km^3 (Larsen and Thorarinsson 1977; Stevenson et al. 2015; Janebo et al. 2016). The hybrid events (type III) represent the majority of the 18 documented historical eruptions, e.g. in 1300, 1693, 1766, 1845, 1947, 1970, 1991, 1980, and

2000. They start with a 30- to 60-min-long explosive phase, subplinian to Plinian in intensity. The opening phase is followed by a sharp drop in magma discharge and a transition into dominantly Strombolian/effusive activity with intense fountaining and relatively fast moving fountain-fed lava flows of icelandite to basaltic icelandite composition (Supplementary document 1). Another sharp drop in magma discharge occurs over the first 1–3 days (Fig. 2), and activity becomes localized to low-altitude vents on the main Hekla fissure or on short radial flank fissures. This activity is typified by Strombolian activity with relatively low discharge rates (<20 m^3 s^{-1}; Table 1).

The repose period of Hekla eruptions and the magnitude of the subsequent eruptions seem to correlate, as a longer repose most often results in a larger and more powerful eruption (e.g. Thorarinsson 1968). During historical times (i.e. since 874 CE), the repose period has ranged from 9 to 120 years with an average of 50 years. The eruptive activity in Hekla before 1947 (including the 1947 eruption) had, on average longer repose, more widespread tephra fall and more voluminous lavas (Thorarinsson 1968). After the 1947 eruption, activity has changed to shorter repose periods and smaller eruptions. Since 1970, Hekla volcano has produced four eruptions, in 1970, 1980 to 1981, 1991, and the last one in February 2000. All were typified by a 0.5–2-h-long opening subplinian phase with discharge ranging from 1100 to 2600 m^3 s^{-1}. In all four events, the sustained and relatively low-discharge (<20 m^3 s^{-1}) Strombolian/effusive phase lasted up to a few months (e.g. Thorarinsson and Sigvaldason 1972; Grönvold et al. 1983; Gudmundsson et al. 1992; Höskuldsson et al. 2007).

The Hekla 1991 eruption

The 1991 eruption was the 17th historical eruption of Hekla. It started on 17th of January 1991 and lasted 53 days, ending on 11th March 1991. Key events of the first 12 h are summarized in Table 1. The onset of the eruption was at 17:01 (Iceland Standard Time); elevated seismicity was first detected 30 min earlier (Soosalu et al. 2003). First observations were of three gas-rich jets, seen from a farm ~50 km WNW of Hekla, accompanied with a faint rumble (Þráinsson 1991). The three jets were seen for ~1 min until a tephra-laden eruption plume started rising from a fissure just north of the 1947 shoulder crater; 5 min later the eruption plume was visible from locations 80 km away from Hekla and it was first detected by radar at 17:10. The opening phase was a 50-min-long subplinian phase producing a 11.5 ± 1.2-km above sea level (a.s.l) high eruption plume in ~10 min, feeding a NE dispersing plume with significant tephra fall up to 370 km from the volcano (Fig. 3). The plume height was estimated by a weather radar of the Meteorological Office and from direct pilot observations (Gudmundsson et al. 1992). The error on measurements
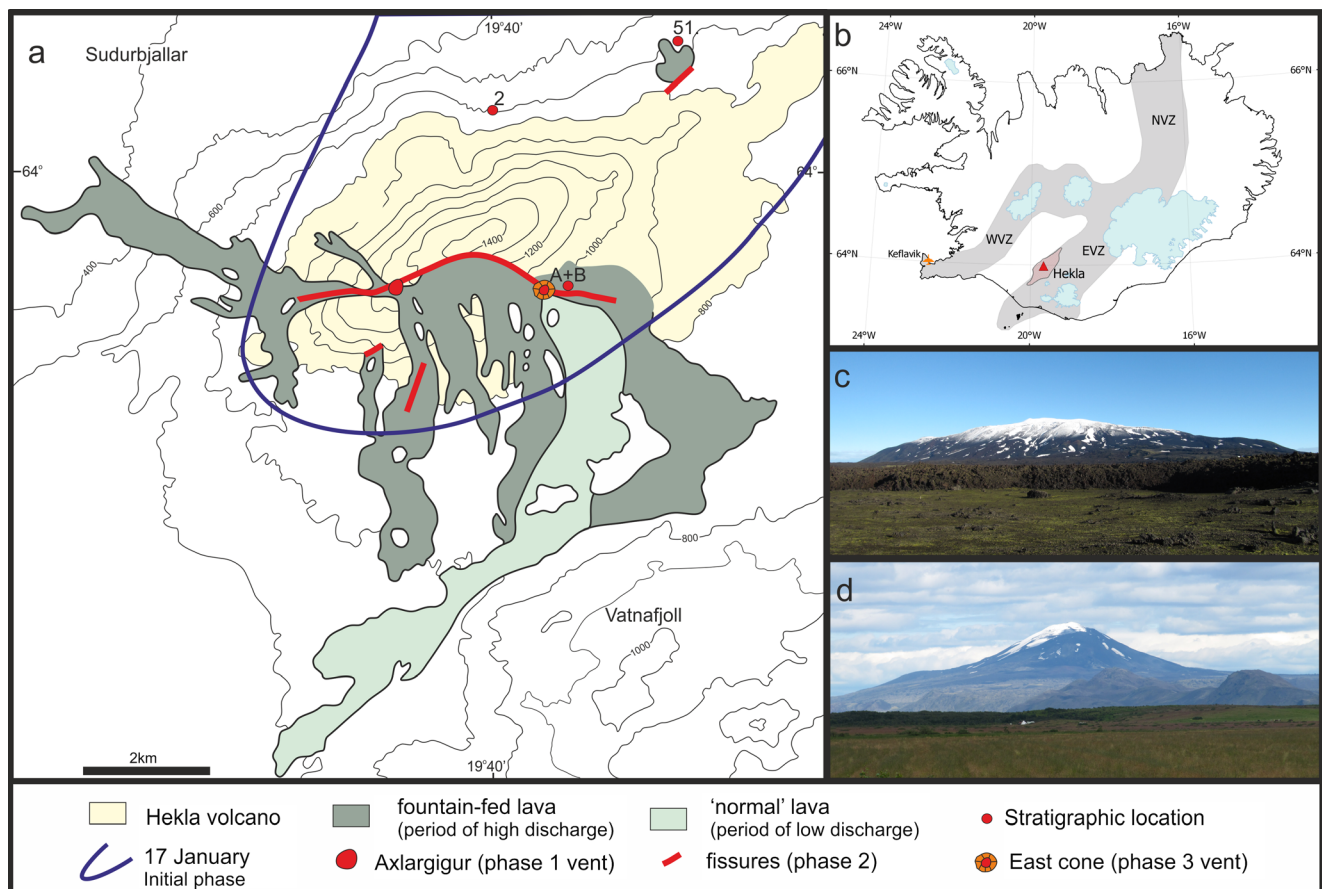
Fig. 1 **a** Distribution map of the 1991 products and active vents (see key for details). Stratigraphic locations indicated are opening phase loc. 51 and 2, transitional phase loc. A+B. **b** Location of Hekla on Iceland (*red triangle*), with the surrounding 720 km² fissure swarm (*outlined*). Also shown is the Western (*WVZ*), Eastern (*EVZ*), and Northern (*NVZ*) Volcanic Zones (*shaded grey*; modified after Sæmundsson 1979). **c** The elongate form of Hekla as seen from the east, perpendicular to the main fissure. **d** The conical form of Hekla as seen from the south along the main fissure

obtained with the weather radar increases with distance and at Hekla it is ±1.2 km (Oddsson et al. 2012). The rise velocity of the subplinian plume was in the range of 20–30 m s^{-1}, whereas the umbrella cloud propagated downwind at velocities of ~20 m s^{-1} (Larsen et al. 1992). A sharp onset of earthquakes at 17:52 marked the start of phase 2 (Table 1), which began with a stepwise opening of the Hekla fissure and the initiation of fountaining that propagated along the opening fissure. This phase of the eruption was typified by 300–500 m high eruptive fountains that fed lava flows that cascaded down the western and southern slopes of the volcano, reaching lengths of 4–5.5 km in <6 h (Fig. 1a). Shortly thereafter, additional fountains emerged from radial northern and southern fissures (Table 1). During the subplinian opening phase (i.e. first 50 min), the magma discharge was on the order of 1260 m³ s^{-1} as calculated from tephra fall deposit volume and duration of the subplinian phase, whereas during the transitional phase 2, the discharge dropped to <50 m³ s^{-1} over the course of 2 days (Fig. 2; Gudmundsson et al. 1992). This decline coincided with an eastward shift and progressive localization of the activity. By the third day of the eruption, the

activity was typified by fountaining on a short fissure segment at the site which became known as the East cone (Fig. 1a). This activity supported only a weak convective plume (<2 km) and represents the switch to phase 3. From this time onwards, the activity was characterized by a single gas-rich fountain, carrying sporadic bombs to heights of several hundred meters with only minor ash. Coarse ejecta gradually accumulated around the vent to form an 80-m high and ~250-m wide scoria cone. At the same time, lava was discharged at rates of 1–12 m³ s^{-1} (Fig. 2 inset), as several flows through separate vents at the base of the East cone (Fig. 1a). The eruption produced, in total, ~0.15 km³ of icelandite lava and 0.02 km³ of tephra fall deposits (Gudmundsson and Sæmundsson 1992; Gudmundsson et al. 1992; Larsen et al. 1992; Supplementary document 1), including a well-defined tephra blanket covering >20,000 km² (Fig. 3; Larsen et al. 1992). The movement of the tephra-laden plume to the NNE was monitored by weather radar, at the Keflavík airport, and tephra fall was constrained visually by residents in the NE part of the tephra sector. Details of the tephra fall from the 1991 eruption are published in Larsen et al. (1992).
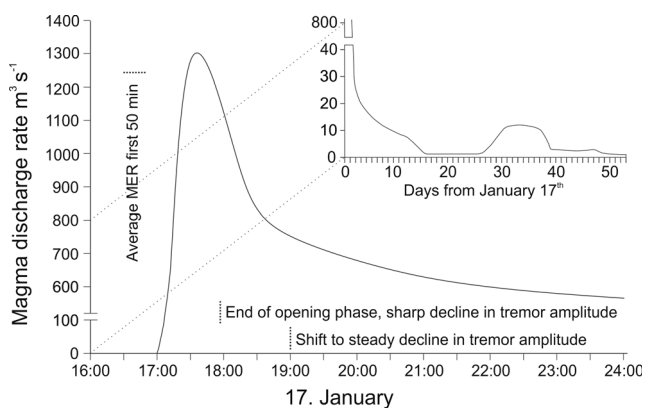
Fig. 2 Diagram showing magma discharge (DRE) versus time for the first hours of the 1991 Hekla eruption. The discharge curve is based on the following: the time averaged discharge during the opening phase, timing of decrease in discharge is based on changes in tremor amplitude (Soosalu et al. 2003), and calculated total output of magma during the first days (Gudmundsson et al. 1992). The *inset* (*top right*) shows the magma discharge during for the rest of the eruption (modified after Gudmundsson et al. 1992)

Methods

Sampling of 1991 tephra fall deposit

The Hekla 1991 tephra fall from the opening phase was sampled during and in the weeks after the eruption (Fig. 3). Within the central highlands, the tephra fall was quickly buried by snow and thus well preserved during the weeks following, although the longer term preservation of the deposit in the medial to distal regions is poor (Larsen et al. 1992). All samples (Supplementary Table 1) were collected from known surface areas (up to 1 m^2) along with entrained snow, which afterwards was melted and decanted off. Sample coverage was increased in 2012–2013, particularly in the proximal sector. The deposit thickness was measured along with mass per unit area and samples were collected for grain-size and vesicularity analysis. The combined 1991 and 2012–13 dataset has good coverage in the proximal and medial sectors, i.e. within the 0.75 kg m^{-3} isomass line, beyond that the coverage drops significantly (Fig. 3). Outer limits of tephra dispersal on 17th of January are well constrained through reports of tephra fall and eyewitness accounts (Larsen et al. 1992).

The key proximal section, location 51, is 5 km from the Hekla summit (Figs. 1a and 3b), and contains the entire proximal tephra fall from the opening phase, preserved beneath the lava flow from the northernmost vent of the 1991 eruption (Fig. 4). Samples were collected through the section, as illustrated in Fig. 5, for grain-size analyses and clast density measurements.

Density

Samples for density analysis were collected at two locations: location 51 (opening phase) and from a site just north of the

East cone (phase 2) (Fig. 1a). Samples from four stratigraphic levels at location 51 represent the subplinian opening phase of the eruption, whereas the two samples (A and B, Fig. 1a) from the East cone are from the transitional phase (phase 2). From each density sample, a set of 100 clasts were measured after Houghton and Wilson (1989). A dense rock equivalent (DRE) value of 2620 kg m^{-3}, calculated using a water pycnometer, was used when converting from measured density to bulk vesicularity.

Grain-size and total grain-size distribution of Hekla 1991

Samples collected for grain-size analyses were manually sieved at half φ intervals down to 4 φ or 63 μm (φ = −log$_2$d, d is the particle diameter in mm). Max diameter (Max$_φ$), median diameter (Md$_φ$ = φ$_{50}$), and sorting coefficient (σ$_φ$ = (φ$_{84}$-φ$_{16}$)/2) were calculated (Inman 1952). Two methods were used to analyse the fine tephra fraction. Firstly, a Beckmann Coulter LS230 at the University of Edinburgh was used to analyse the fraction finer than 1 mm. The output was binned in half φ intervals and combined with the sieving data based on mass finer than 1 mm in the sample, and the overlap of data from 1 mm to 63 μm was used to validate the data sets. Secondly, a SediGraph III at the University of Iceland was used to analyse the fraction smaller than 250 μm. The SediGraph uses horizontally collimated beam of X-rays to measure relative particle mass concentration in a liquid medium. The SediGraph then applies Stokes Law to determine relative percentage in each size class under known liquid conditions (density and viscosity) and known particle density (2620 kg m^{-3}). The output was binned in half φ intervals and combined with the sieving data based on mass finer than 250 μm in the sample. The data overlap from 250 to 63 μm was used to check if sieving and mechanical analyses gave consistent results. TGSD was calculated using a total of 26 samples, mostly from within the 0.75 kg m^{-2} isomass line (Fig. 3). All samples used for TGSD calculation are bulk samples, at location 51 (Fig. 1) where stratigraphic sampling was done, bulk sample of the deposit was collected for the TGSD calculation. The zero deposit line was determined from eyewitness accounts of tephra deposition on 17th of January (Fig. 3). The TGSD was determined by the Voronoi Tessellation method of Bonadonna and Houghton (2005), using an updated version of the code (Biass and Bonadonna 2014). This method assigns a polygonal Voronoi cell (see Supplementary Fig. 1) to each sample and the TGSD of the deposit is obtained as the area-weighted average of all the cells covering the deposit. Criteria for sample selection were to optimize deposit coverage. This method has successfully been applied to other eruptions where sampling was contemporaneous with eruption, e.g. the 1996 Ruapehu eruption, New Zealand

Table 1 Sequence of events of during the first hours of the Hekla 1991 eruption, summarizing phases 1 and 2 on 17th January to 18th January (Gudmundsson et al. 1992; Larsen et al. 1992; Linde et al. 1993; Soosalu et al. 2003)

Time	Seismicity	Eruptive vents	Interpretation
16:32	First volcano-tectonic earthquakes detected, growing in intensity (ML = 1–2) and frequency to 17:00. Strain contraction starts		Intrusion of magma rising through the Hekla conduit system. The magma travelled from holding chamber to the surface in ~30 min
17:01	Onset of volcanic tremor, which remained at high intensity levels to ~18:00	Three large gas jets rise emerge from a short fissure near the 1947 Shoulder Crater	Onset of visible eruption
17:02		Black tephra-laden column emerges from Shoulder Crater fissure	Appearance of subplinian column, start of phase 1
17:05–17:07		Rapidly rising eruption column at Hekla seen from several farms in S-Iceland. As its top decelerated it spread out before being deflected northwards by wind	Eruption column rising vertically above Hekla and forming a small umbrella cloud before downwind dispersal of the plume (to north)
17:10		Eruption plume first detected by the Iceland Meteorological Office weather radar, column and plume height ≥11.5 km	Fully developed eruption column constructed at rise velocities in the range of 20–30 m s^{-1}
17:52	Relatively strong earthquake (ML = 2.5)	Lava fountains appear from the Shoulder Crater fissure, signalling the onset of simultaneous explosive and lava fountain eruption	Termination of subplinian eruption (phase 1) and the initiation of phase 2. Duration of phase 1 = 50 min
18:00	Volcanic tremor decreases sharply between 18:00–19:00 h	Intense explosive activity on a new fissure down slope from Shoulder Crater fissure, propagating westward at the time and featuring a line 300–500 m high fountains supporting a 12 km high eruption column (as measured by Iceland air pilots in transit). Also, a new short fountaining fissure opened on the north flank of Hekla	Opening of the Hekla fissure with fire fountain activity on lengthening fissures marking a full transition to phase 2
18:06–18:40	Series of relatively strong earthquakes (ML = 2.0–2.3), lasting for 24 min (18:06 to 18:30), followed by sharp decrease in earthquake intensity and frequency over 40 min. Strain contraction stops at 18:40	Lava fountains first seen on radial fissures on south slope of Hekla, followed by a gradual lengthening of the Shoulder crater fissure and stepwise propagation of explosive and lava fountain activity, first to the NE along the crest of Hekla towards the Summit Crater and from there eastward, diagonally down the eastern slope of Hekla	Evolution of phase 2 activity marked by continued growth and lengthening of the Hekla fissure to the NE and associated explosive and lava fountain activity
19:00–20:00	Continued but gradual decrease of volcanic tremor. Slight increase in earthquake intensity and frequency from 19:05–19:40, followed by a 2-h-long period steady decline	Renewed growth of the phase 2 eruption plume close to Hekla volcano	Slight increase in phase 2 activity
20:00–21:00	Continued decline of seismic activity	Decreasing explosivity, with a lull in explosive activity around 21:00. Phase 2 eruption plume detached from the volcano at 20:50	Gradual temporary decrease in phase 2 activity
21:30–24:00	At 21:32: Relatively strong earthquake (ML = 2.3)	Eruption intensity decreases rapidly on SW-part of the Hekla fissure. Eastward lengthening of the Hekla fissure (at ~900 m a.sl.), coupled with renewed vigour of the activity on the segment of Hekla fissure that extends from the Summit Crater to the foot of the eastern flank	Renewed vigour of phase 2 activity in junction with a shift of the vents to NE part of the Hekla fissure
0:00–4:00	Earthquake intensity and frequency and volcanic tremor decrease at steady rate	Strong explosive and lava fountaining activity, of gradually decreasing intensity, continued into the night on NE part of the Hekla fissure	Intensity of phase 2 activity begins to drop off leading to gradual localization of the eruptive vents
>4:00	Volcanic tremor levels off to low but steady intensities and earthquakes taper off	Activity characterized by rapid decrease in eruption intensity coupled with progressive localization of the eruptive vents onto a short fissure segment at the foot of the east slope (i.e. at the site of the East Cone (= phase 3 vent))	Waning stages of phase 2 activity leading to the transition to phase 3 on 20 January. From then on, activity was confined to the East Cone vent and characterized by weak Strombolian explosions and quiet effusion of lava

Fig. 3 Isomaps of the Hekla 1991 deposits. The *top panel* shows the extend of the 1991 tephra fall on land with isomass (kg m^{-2}) lines. Outermost limits of tephra fall are after sampled tephra and reports from the eruption. *Lower panel* shows the isomass (*far left*), isopach (*centre*), and isopleth (*far right*) maps for the proximal and medial sectors of the fall deposit. Based on Larsen et al. (1992), with additions from unpublished 1991 field data (Thordarson and Larsen) and new field observations in 2012 and 2013 by principal author
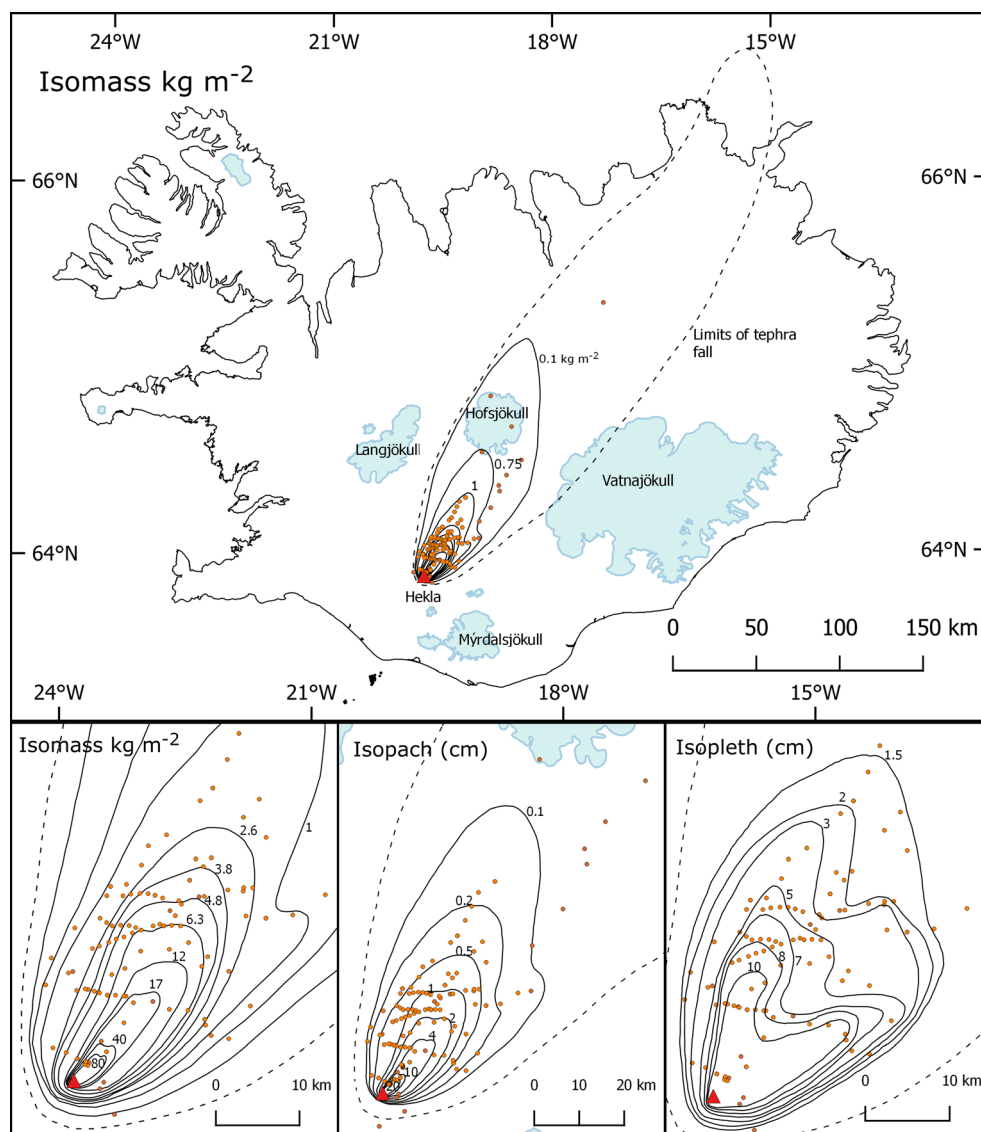
(Bonadonna and Houghton 2005), and the 2001 and 2002–03 eruptions at Mt. Etna, Italy (Scollo et al. 2007; Andronico et al. 2008).

Volume and mass of deposit

The volume of erupted tephra was calculated by integrating best fit lines on semi-log plots of deposit thickness and mass per unit area versus square root of area using multiple exponential segments (Fierstein and Nathenson 1992; Pyle 1989): power law (Bonadonna and Houghton 2005) and Weibull (Bonadonna and Costa 2012) functions. Transformation from mass per unit area to equivalent thickness for the data collected in 1991 was done using measured bulk densities from 400 to 940 kg m^{-3} (Larsen et al. 1992).

Plume height and mass eruption rate

Average mass eruption rate (MER) was calculated from the known duration of the opening phase and the calculated mass of the tephra deposits. In addition, to account for strong wind during the eruption, MER was calculated using the method of Degruyter and Bonadonna (2012). Magma temperature was varied according to magma composition from 1173 to 1373 K, the plume heights measured by the weather radar were used 8.8, 10, and 11.2 km above vent (10.3, 11.5, and 12.7 a.s.l., respectively) but wind speed was kept constant at 20 m s^{-1}, and the wind- and radial-entrainment coefficients were set to 0.5 and 0.1, respectively. The scaling parameter Π was also calculated to give insights into plume dynamics (Supplementary Table 2; Degruyter and Bonadonna 2012). Maximum plume height (*H*) was observed but was also calculated using the empirical relationships $H = 1.67\, Q^{0.259}$ (Sparks
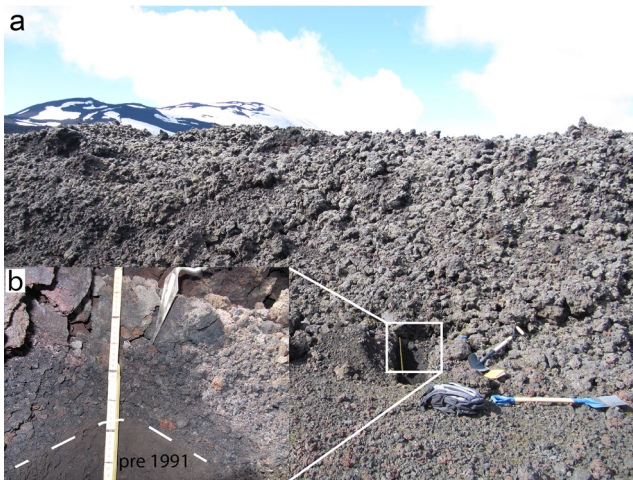
Fig. 4 a Location 51, the principal stratigraphic for the Hekla 1991 deposit (see Fig. 1 for geographic location). Photo taken on 27th of July 2012. At this site, the fall deposit is partly overlain by a small lava flow from the 1991 eruption. This site was chosen to ensure sampling of the Hekla 1991 fall deposit and not the subsequent Hekla 2000 event. **b** The deposit is 15 cm thick at location 51, the fine grained base in the image is pre 1991 and the larger grains at top are from the lava on top. *Black lines* on measuring stick are 5 cm apart

et al. 1997) and $H = 2.00 \, Q^{0.241}$ (Mastin et al. 2009) (based on 34 historic eruptions, including the 1947, 1970, and 1980 Hekla events) where Q is the time-averaged MER.

Results

The 1991 tephra fall deposit—physical characteristics and dispersal

In the proximal region, up to 7 km from source, the 1991 deposit is made up of metallic bluish black scoria bombs and lapilli, and is poor in wall-rock lithics but with minor amounts of red cored bombs. Bombs are only common in the most proximal Hekla deposits. These bombs are fragile and have expanded after fragmentation with a concentration of very coarse vesicles in the cores. Beyond 7 km from source, the deposit is ash dominated.

The tephra dispersal from the subplinian phase forms a narrow (max 70 km wide) sector with the main dispersal axis trending NNE and a less distinct, secondary axis to the NE. The tephra thins rapidly along the dispersal axis; thinning half distance for the deposit is 5.5 km. At 13 km downwind of Hekla, the cross-wind half-distance is 3–4 km. The isomass and isopach contours are almost identical while the isopleth is crudely bilobate (Fig. 3), with two axes in the proximal area.

Two principal subunits were identified, described, and sampled at location 51 (Figs. 1, 5, and 6). Further away from Hekla, where deposits are <5 cm, subunits were not recognizable. At location 51, the basal subunit is a 7.5-cm-thick,

very poorly sorted (σ_φ 2.1–2.9), inversely graded, lapilli-dominated fall. The basal subunit is overlain by a 0.5-cm-thick finer grained layer of medium to coarse ash, containing poorly sorted (σ_φ 1.3) fluidal and blocky juvenile clasts (Fig. 7). The overlying top subunit resembles the basal one; it is a 7-cm-thick, inversely graded, poorly sorted (σ_φ 1.4–1.7), clast-supported lapilli-dominated fall (Fig. 5). The tephra is homogeneous in terms of juvenile clast properties and the top subunit is distinctly lithic-poor. Lithic content in the basal sample (sample 8 in Fig. 5) is highest around 5% at −1.5 φ but averages around 1% of mass in the range −3 to 0 φ. Sample 7 is poorer in lithics. The lithic population is dominated by dark fragments of aphyric lava, with minor amounts of highly altered, light coloured, and red lava fragments.

Grain-size distribution

The grain-size distribution of individual samples is generally unimodal and show variation in maximum, minimum, and modal grain-size depending on distance from vent (Fig. 8a). However, bimodal grain-size samples are present, with the secondary peak in the <2 mm fraction. Sorting ranges from very well to poorly sorted (σ_φ 0.7 to 3; Fig. 8b) and median diameter ranges from −3.9 to 4 φ.

At location 51, the four grain-size samples from the lapilli fall units (Fig. 5) are bimodal whereas the grain-size sample from the ash layer (sample 6 in Fig. 5) is unimodal.
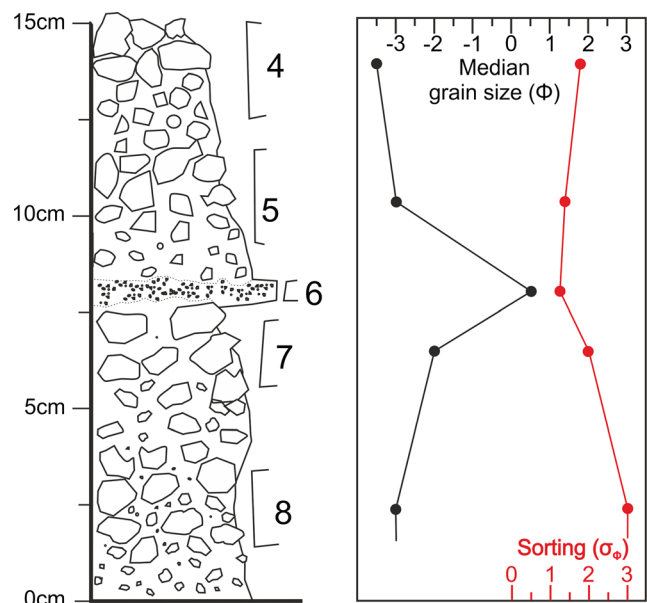

Fig. 5 Stratigraphic log of the Hekla 1991 tephra fall deposit at locality 51. Two principal fall units are identified separated by 0.5 cm thick parting of medium to coarse ash. Samples were collected for grain-size and density analyses. Grain-size samples were collected in subunits, samples (J12-51) 4–8 and density samples for 4, 5, 7, and 8. Sorting calculated after Inman (1952)

Fig. 6 Histograms showing the clast density measurements from both subunits (samples J12-51 4 to 8) at location 51. Also shown are clast density measurements from phase 2 tephra fall (samples H1991-A and B from the east cone location; Fig. 1a). The span in clast density is narrow, ranging from 520 to 880 kg m^{-3} and each sample exhibits a tight unimodal and log-normal distribution indicating a mean vesicularity of 77 to 79% for the analysed pumices, obtained via conversion of clast density using melt density of 2620 kg m^{-3}. Samples were analysed after the procedure of Houghton and Wilson (1989). Note, samples J12-51 4, H1991 A and B feature the tightest distributions
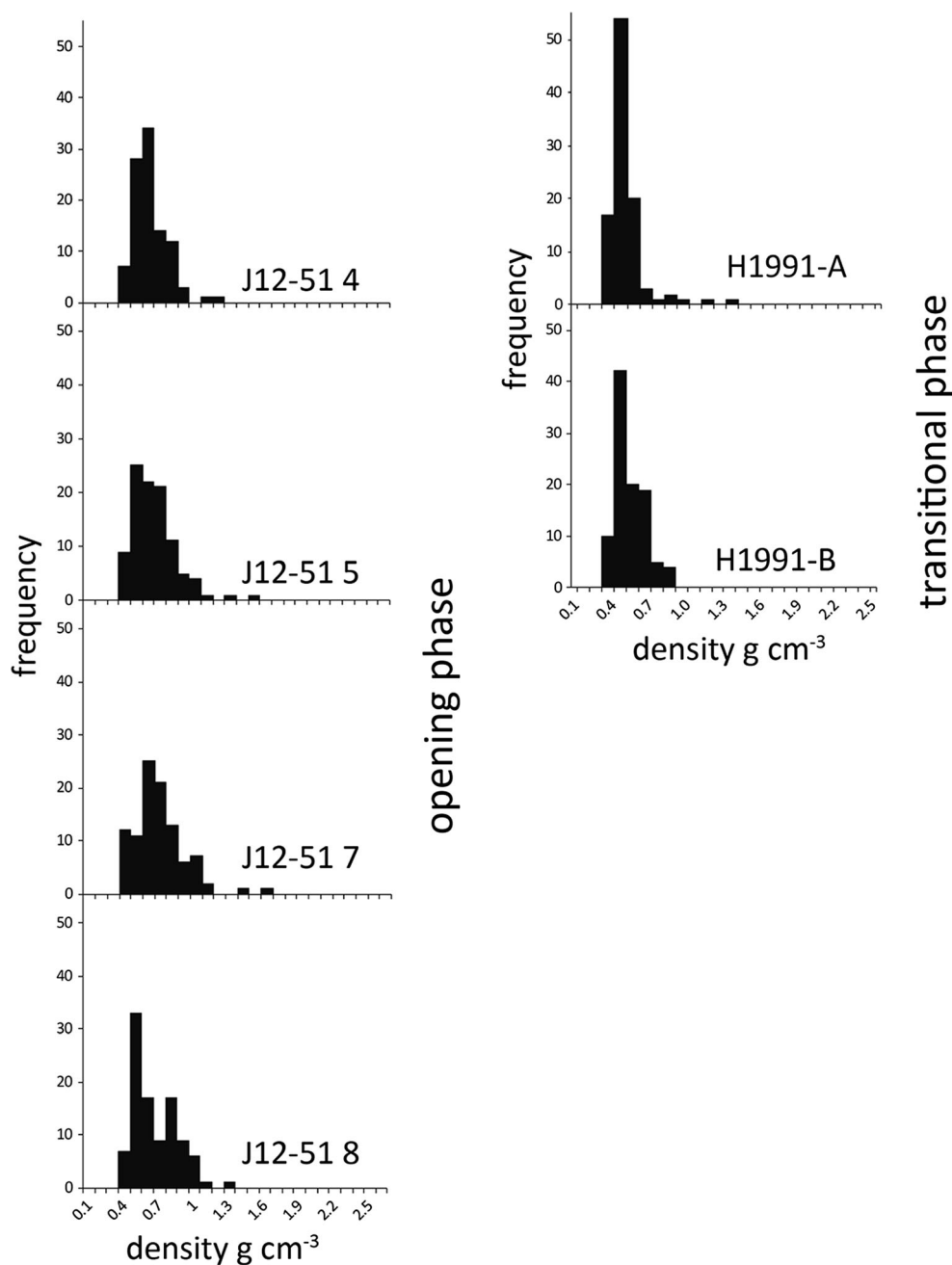
The bimodal samples have a primary coarser mode at −3.5 to −2.5 φ and a secondary finer mode at 3 to 4 φ (Fig. 5). There is a slight upward coarsening along with better sorting and lesser amounts of ash (<2 mm) in samples 4 and 5, compared to in samples 7 and 8 (Fig. 9). Samples 4 and 5 have Md$_\varphi$ −3.5 to −3 φ and are better sorted (σ$_\varphi$ 1.4 to 1.7) than samples 7 and 8 which have Md$_\varphi$ −3.1 to −2.6 φ and σ$_\varphi$ 2.1 to 3.

Along the main depositional axis, a size fractionation induced by transport and deposition becomes apparent. Samples along the main depositional axis show size fractionation with distance of the primary coarse mode (samples closer than 82 km, Fig. 8a). The two most proximal samples show slight bimodality, relatively broad coarse peaks at −3.5 and −1.5 φ, and smaller fine peaks around 3.5 φ. Bimodality is also seen in the medial samples (38, 52 km), sharper coarse peak at 0 to 2 φ and smaller finer peaks around 3.5 φ. Distal samples (82, 115, and 195 km from source) show only a broad fine peak at 3.5 to 4.5 φ (Fig. 8a). Another noteworthy feature is the small change of the grain-size mode of samples from 82 to 195 km from source (Fig. 8b), whereas over the same distance isomass values drop from 0.75 to 0.1 kg m^{-2} (Fig. 1a). Deposition of lapilli (64–2 mm;
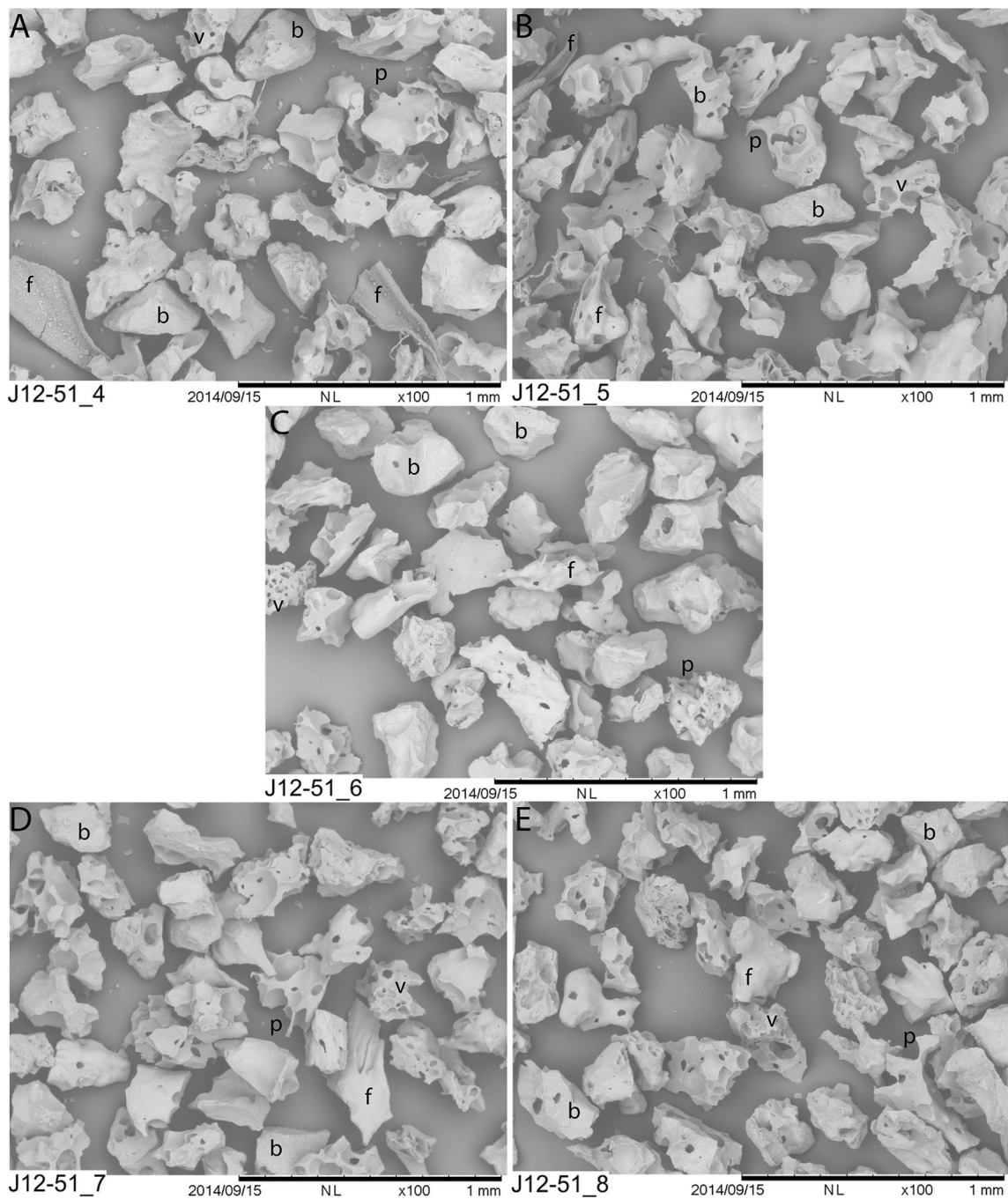
Fig. 7 Scanning electron microscope (SEM) images of grain-size samples from location 51. Grains were selected from the 2.5 φ bin in order to examine the finer grain-size peak observed in Fig. 9. Samples are shown in stratigraphical order from top left to bottom right. These moderately to highly vesicular ash grains have viscous fluidal or blocky shapes. The fluidal (*f*) grains typically have smooth shiny outer surfaces, which in some instances feature smaller sub-ten micron grains adhering to their surface (e.g. a. sample J12-51-4 grains at bottom left and right). The blocky (*b*) grains feature pristine curvi-planar surfaces typical of brittle fracturing. These grains also preserve small delicate protrusions (*p*) that have survived the transport through and deposition from the eruption plume

−6–1 φ) is concentrated during the first 25 km when it is the dominant grain-size (>60 wt%). From 25 km onwards, coarse ash becomes the dominant grain-size in the deposit, and fine ash becomes an important part of the deposit after 70 km. Changes in grain-size Md_φ, Max_φ, and σ_φ with distance from source (Fig. 8b) show that the most scatter for all parameters occur in the first 15 km. There is a steady decrease in Md_φ and Max_φ from ~0 to 65 km and then almost constant values from 65 to 195 km, where coarse ash is the dominant component (Fig. 8c). Over the same distance, σ_φ improves significantly out to 20 km and then shows no further significant variation.
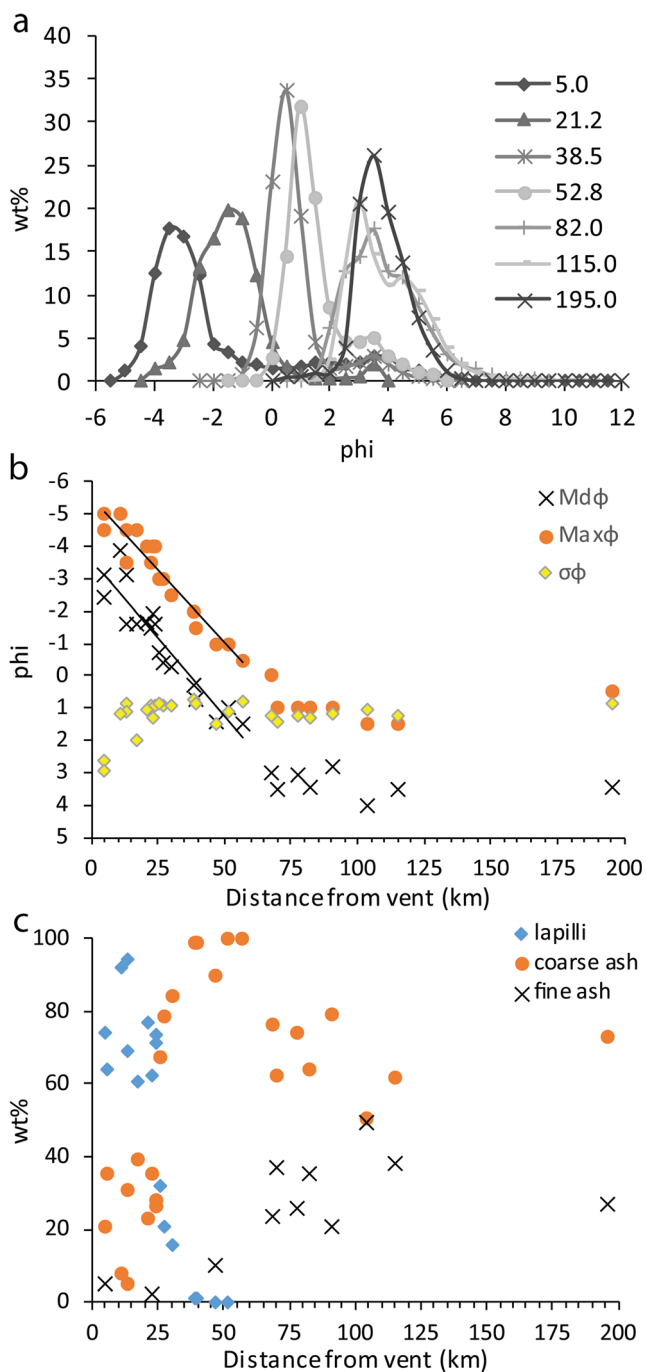
Fig. 8 a Grain-size distribution of selected samples along the principal dispersal axis of the Hekla 1991 tephra fall. *Each line* represents a sample at indicated distance from Hekla. **b** Variation of Md_φ, Max_φ, and sorting (σ_φ) of all Hekla 1991 grain-size samples as a function of distance from vent. Two lines show best fit through Md_φ and Max_φ data from 5 to 57 km from source. **c** Comparison of relative abundance of lapilli, coarse ash and fine ash with distance from source. Lapilli 64–2 mm, -6–1φ; coarse ash 2–0.063 mm, -1–4φ; fine ash <0.063 mm, >4φ

Total grain-size distribution

The TGSD (Fig. 10) is bimodal with a primary mode at -3.5 to -2.5 , and a secondary mode at 2.5 to 3.5 φ. Md_φ is -1.8 φ

and σ_φ is 3.3. The ash fraction (<2 mm; $\geq -1\varphi$) amounts to 37% of the tephra mass, but fine ash (<63 µm; $\geq 4.5\varphi$) accounts for only 6%.

Clast density

The density measurements of the 1991 pyroclasts show tight density/vesicularity distributions up through the type 51 section (Fig. 6). The range of mean clast density is 550 ± 140 to 600 ± 210 kg m^{-3}, corresponding to calculated mean vesicularities of 78 to 75%. The maximum measured juvenile clast density is 1520 kg m^{-3}, corresponding to a minimum vesicularity of 42%, while the minimum clast density is 310 kg m^{-3}, indicating a maximum vesicularity of 88% (Table 2). The density/vesicularity distributions are unimodal and weakly skewed towards higher densities, or lower vesicularity, with a standard deviation in the range of 140 to 210 kg m^{-3} for clast density and 5 to 8% for vesicularity (Fig. 6; Table 2). From the East cone location (Fig. 6, Table 2), samples H1991 A and B range in mean clast density from 520 ± 120 to 480 ± 150 kg m^{-3}, corresponding to calculated mean vesicularities of 80 to 81%. The maximum measured density is 1310 kg m^{-3}, which corresponds to a minimum vesicularity of 50%. The minimum clast density is 310 kg m^{-3}, corresponding to maximum vesicularity of 88%. The density/vesicularity distributions are unimodal, and less skewed towards higher densities than samples from location 51 with standard deviation of 120–150 kg m^{-3}, or 5–6% vesicularity (Fig. 6; Table 2).

Eruptive parameters

The estimates of volume of tephra fall from the opening phase using the three integration techniques ranges from 0.016 to 0.019 km^3 (Fig. 11a). The three-segmented exponential method gives 0.019 km^3, the power law 0.019 km^3, and the Weibull function 0.018 km^3, a difference of 0.001 km^3. The estimate of erupted mass derived by fitting three exponential segments (Fig. 11b) is 9.9×10^9 kg, the Weibull method gives 8.6×10^9 kg, whereas the power law results in 9.6×10^9 kg (corresponding to tephra volumes of 0.020, 0.017, and 0.019 km^3, respectively, using bulk density of 500 kg m^{-3}). The slightly lower values obtained here than the original estimate of 0.022 km^3 (Larsen et al. 1992) are due to the new mapping that better constrains thickness in the proximal area. The result from the integration using isomass data is considered the most reliable approaches to mass estimation of the opening phase, as no conversion to thickness is needed. All methods provide excellent fit to the data points (exponential $r^2 = 0.96$ to 0.98, Weibull $r^2 = 0.99$, and power law $r^2 = 0.97$). Here, the results from the Weibull are preferred as the most conservative estimate.

Using the estimates of 8.6×10^9 and 9.9×10^9 kg (0.003 and 0.004 km^3 DRE; Weibull and exponential, respectively),
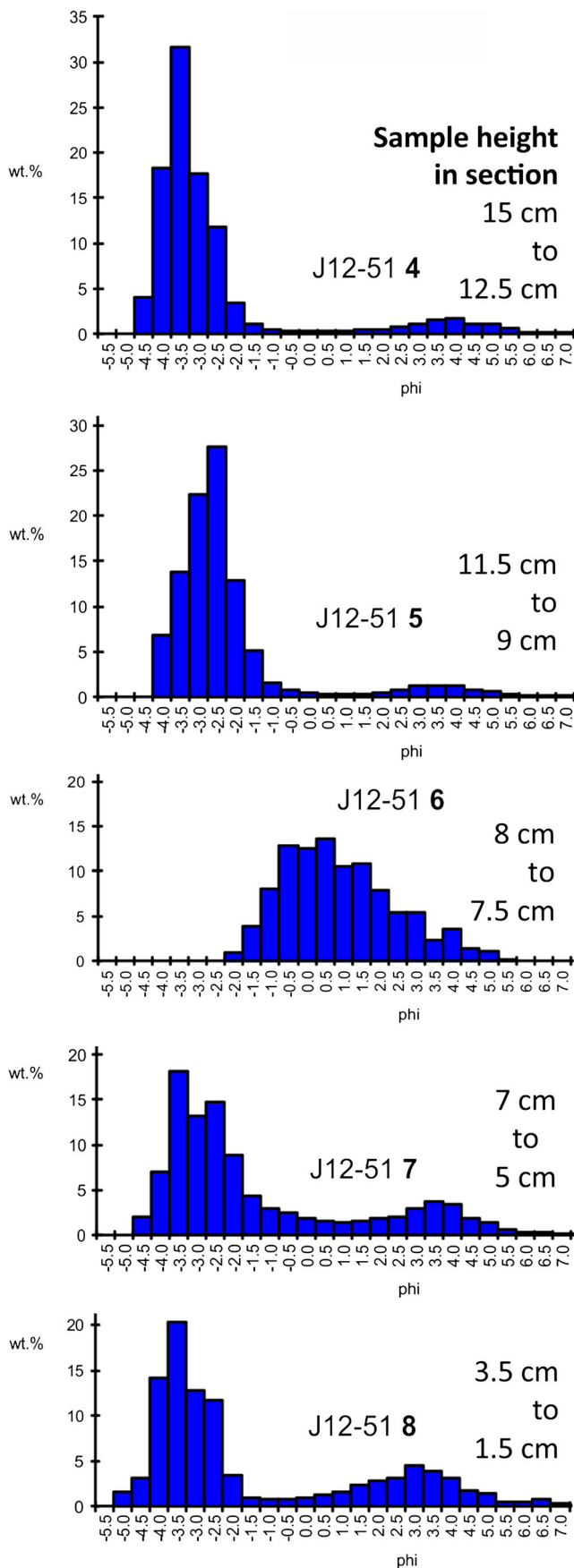
◀ **Fig. 9** Grain-size analyses for samples collected at location 51. Samples are bimodal except sample J12-51 6, the bimodal samples have principal coarse peak at −3.5 to −2.5 φ. The finer peak is at 3 to 4 φ. The lower fall unit (samples 7 and 8) has on average less defined coarse peak and higher mass contribution from the fine peak compared to the upper fall unit (samples 4 and 5)

the calculated time-averaged MER is between 2.9×10^6 and 3.3×10^6 kg s^{-1}. Conversion to volumetric MER, using DRE of 2620 kg m^{-3}, results in values of 1100 to 1260 m^3 s^{-1}. Plume heights empirically derived from the MER are 12 to 12.4 km a.s.l. (Mastin et al. 2009). This is in good agreement with the 11.5 km a.s.l. plume reported by Gudmundsson et al. (1992) and Larsen et al. (1992). Calculating the MER after Degruyter and Bonadonna (2012), and using the measured plume height by the radar (10 ± 1.2 km above vent), and wind speed of 20 m s^{-1} (Larsen et al. 1992), results in MER of 3.4×10^6 to 1.6×10^7 kg s^{-1} and scaling parameter Π of 0.20 to 0.26 (Supplementary Table 2).

Eruption type

The calculated maximum deposit thickness from the semi-log plot is 35 cm (Fig. 11a), and the thickest measured section is 28 cm. Following Walker (1973), the calculated dispersal index (D) is 460 km^2, and the fragmentation index (F) is 6.3%. These values are consistent with an explosive phase of subplinian intensity. Both the deposit volume and plume height would classify the eruption as a VEI 3 (Newhall and Self 1982) and the plume height equates to the M3 category of Mastin et al. (2009). However, using more recent classification methods that combine plume height with MER, the opening phase falls into the small to moderate category below the field of subplinian events (Bonadonna and Costa 2013).

Discussion

Explosive Hekla eruptions

Of the known post glacial explosive eruptive activity in Hekla, the 1970, 1980, 1991, and 2000 eruptions have produced the smallest volume of tephra fall and weakest intensity events (Fig. 12). Other historic Hekla (type III) eruptions are larger than the 1970 to 2000 activity, but smaller than the e.g. 1104 CE and H4 (type II) Hekla eruptions (Fig. 12; Larsen and Thorarinsson 1977; Thorarinsson and Sigvaldason 1972; Grönvold et al. 1983; Gudmundsson et al. 1992; Höskuldsson et al. 2007; Janebo et al. 2016). The 1991 eruption and other post 1947 Hekla eruptions are strikingly similar in sequence of events, composition of erupted materials, and eruption source parameters (Fig. 12; Supplementary document 1; Thorarinsson and Sigvaldason 1972; Grönvold
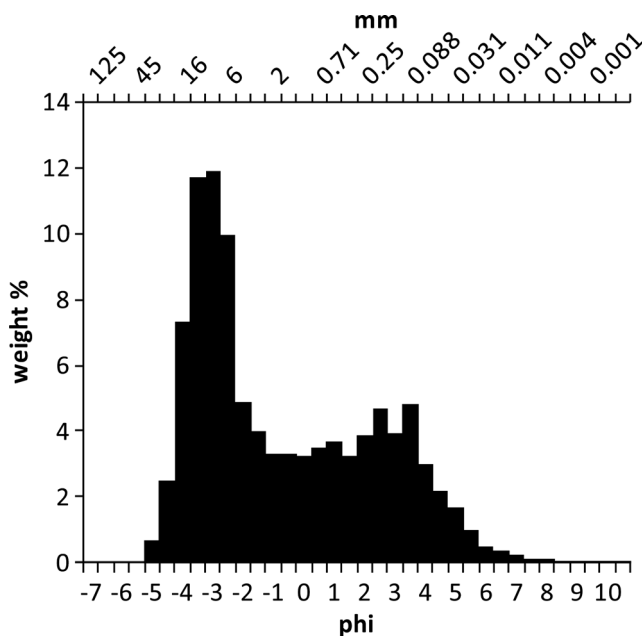
Fig. 10 Reconstructed TGSD of the opening phase tephra fall from the Hekla 1991 eruption. Note the bimodal distribution. The tighter coarse peak is around −3.5 to −2.5 φ, while the finer peak is broader, extending from around 2.5 to 3.5 φ. Spatial distribution of samples included in the calculation is shown in Supplementary Fig. 1

et al. 1983; Gudmundsson et al. 1992; Lacasse et al. 2004; Höskuldsson et al. 2007). But as illustrated here, there is potentiality for complex eruption dynamics in these short and smaller events.

Proximal tephra fall deposits

The threefold stratigraphy observed in the proximal tephra fall deposits, i.e. two coarse lapilli-dominated fall units separated by an ash parting as seen at location 51 (Fig. 5), cannot be explained by continuous deposition from a steadily rising and spreading plume. A plausible interpretation is that the opening phase of the eruption featured two distinct explosive phases, separated by a long enough break for the 0.5-cm-thick ash layer to accumulate. However, syn-eruptive observations as reported in Larsen et al. (1992) and tremor data (see Figs. 3 and 4 in Soosalu et al. 2003) do not indicate any pause in

activity during the opening phase, rendering the above explanation unlikely.

At the most proximal site measured on 23 January 1991 (location 2, Fig. 1a), two lapilli fall units, which we interpreted to be the two beds at location 51, were separated by 4–5 cm of newly fallen snow. This suggests a short but distinct break in the lapilli accumulation.

We therefore suggest that the opening phase had a pulsating source with sustained atmospheric plume. Between the lapilli fall units, finer particles were aggregated by snow and deposited. Snow-induced aggregation may furthermore be the source for bimodality observed in the lapilli fall units (Fig. 9). Aggregation by snow commonly occurs in Iceland, e.g. in the 2000 Hekla eruption (Lacasse et al. 2004), the 2010 Eyjafjallajökull eruption (Thordarson, unpublished data), and in the 2011 Grímsvötn eruption (Gudnason, unpublished data).

Bilobate proximal isopleth lines (Fig. 3) indicate shift in wind direction during the opening phase, the bilobate shapes are not recognized in other isolines (Fig. 3). Indicating a relatively short temporal shift in wind direction, shift that is only recorded by large clasts, and thus not long enough to alter the general trend of the isopach map (Fig. 3). A more general shift in wind direction was recorded during the eruption, data from the weather radar indicates that the plume at 2 km a.s.l did shift from NNE at 17:50 to ENE at 23:50 (Larsen et al. 1992).

The reverse grading of each lapilli unit can be explained either by increasing eruption intensity and thus deposition from higher altitudes, or by shifts in the wind direction. Bilobation in the most proximal isopleth lines (Fig. 3) support wind shift. However, for two reversely graded fall units, wind shifts would need to be two. For the duration of the opening phase, that is not considered plausible. However, the reverse grading could be combination of the two, i.e. shift in wind direction and/or increasing eruption intensity.

Shallow conduit processes

The density data (Fig. 6) show minor variation over stratigraphic level (i.e. time). The lower lapilli unit at location 51 starts with a broad, slightly bimodal distribution that with time
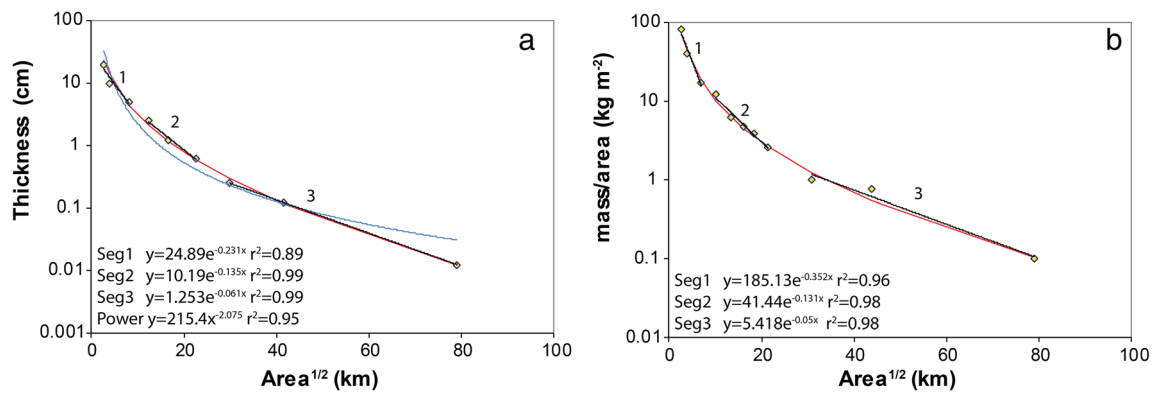
Table 2 Vesicularity/density results from location 51 and the east cone. Four samples were analysed from location 51, stratigraphic height is illustrated in Fig. 9. Two samples from the east cone location were analysed (samples H1991 A and B)

	J12-51 4	J12-51 5	J12-51 7	J12-51 8	H1991-A	H1991-B
Mean vesicularity	78%	75%	75%	76%	80%	81%
Standard deviation	5%	8%	8%	7%	5%	6%
Maximum vesicularity	87%	88%	88%	88%	87%	88%
Minimum vesicularity	56%	42%	42%	52%	66%	50%
Mean density	0.55	0.57	0.6	0.59	0.52	0.48
Standard deviation	0.14	0.19	0.21	0.18	0.12	0.15
Maximum density	1.15	1.44	1.52	1.25	0.9	1.31
Minimum density	0.33	0.32	0.31	0.31	0.36	0.31

Fig. 11 Thickness vs √Area and mass per unit area vs √Area for the tephra fall deposit of the Hekla 1991 opening phase. Area of each isoline indicated by *yellow diamonds*. The data can be taken to define three exponential segments (*black solid lines*), best fit Power law solution (*blue dotted line*), and Weibull fit (*red solid line*). Equations for exponential fit, power law fit, and r^2 are shown in the lower left corner of each diagram

becomes unimodal. The upper lapilli unit shifts towards a narrower distribution over time. The broader initial density distribution is possibly due to partly degassed magma (i.e. gas flames in start of eruption), responsible for opening the conduit. The narrower density distributions towards the end of the opening phase indicate more stable conditions for vesiculation in the shallow conduit. Broad density distributions are thought to reflect heterogeneous textures in the magma, which could reflect heterogeneous vesiculation/degassing condition in the shallow conduit (e.g. Houghton et al. 2004). This could be linked to variation in rise speed during opening of the conduit in 1991, and resulting in less supersaturation and/or more loss of volatiles along the conduit walls. The somewhat narrower density distribution (samples 4 and 5; Fig. 6) is formed when the conduit is better established and less variation in ascend speed across conduit can be expected. Although interpretations of density data are only speculative without vesicle size distributions, it seems likely that throughout the opening phase of the 1991 eruption, vesiculation conditions became increasingly homogeneous. These conditions then continued in phase 2 of the eruption (as shown by the samples from the East cone location). This, together with the overall intensity decrease (Fig. 2) indicate that magmatic volatiles rose coupled to the magma in the beginning of the eruption but with time became decoupled as intensity decreased.

Eruptive parameters

The mass of tephra deposited during the opening phase of 8.6×10^9 kg reflects fine spatial resolution in the proximal and medial areas, and coarse resolution in the distal area. In fact, the most distal isomass contour is only constrained by
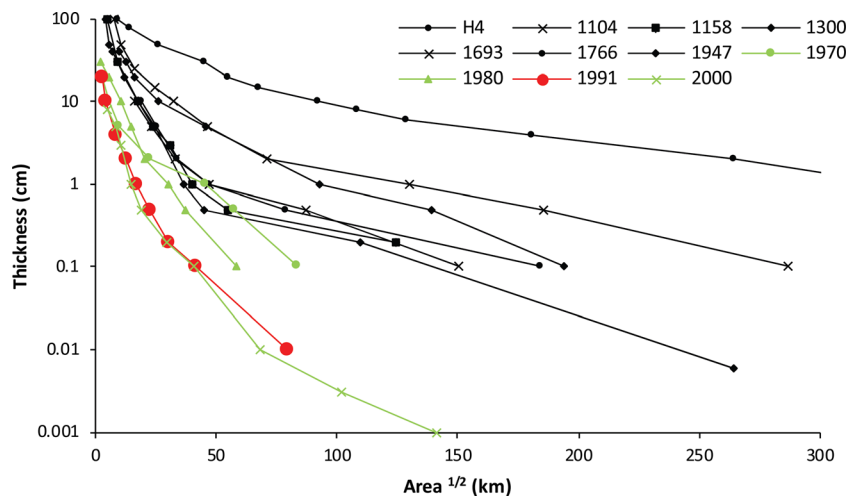

Fig. 12 Thickness vs √Area for selected post glacial explosive Hekla eruptions. Legend indicates year of eruption for all but H4 which is a ~4300-year-old event. *Black lines and symbols* are pre 1970 eruptions. *Green* are the 1970, 1980 and 2000 eruptions, and in *red* the 1991 eruption. Sources for thickness and area data: H4 from Larsen and Thorarinsson (1977), 1104 to 1766 from Janebo et al. (2016), 1947 from Thorarinsson (1968), 1970 from Thorarinsson and Sigvaldason (1972), 1980 from Grönvold et al. (1983), 2000 from Haraldsson (2001), and 1991 from this study

one point on the downwind side (Fig. 3a). Mass estimate of the tephra fall deposits without this 0.1 kg m^{-2} results in larger apparent mass for both exponential and Weibull fits (9.1 to 9.6 × 10^9 kg).

The MER (2.9 × 10^6 kg s^{-1}) obtained from the mass of the deposits and the duration of the opening phase is a time average value, although the empirically derived plume heights are in good agreement with observations in 1991 (Gudmundsson et al. 1992). The strong wind during the eruption affected tephra fall (Fig. 2) and likely decreased the plume height. The method of Degruyter and Bonadonna (2012), which takes the effect of wind into account, indicates that even a plume height of 10.3 a.s.l. would correspond to a MER of 3.4 to 4.3 × 10^6 kg s^{-1} whereas the reported plume height of 11.5 km a.s.l. would correspond to a MER of 6.9 to 8.6 × 10^6 kg s^{-1}, and plume height of 12.7 km a.s.l. results in MER of 1.3 to 1.6 × 10^7 kg s^{-1} (Supplementary Table 2). This indicates that at peak discharge in 1991 the MER was higher than the time averaged and the wind field did affect the ability of the eruption plume to rise fully. Nonetheless, the MER calculated from a 11.5-km a.s.l. high plume is probably at the higher end for Hekla 1991, as pilots and the weather radar report this altitude. Also Hekla eruption plumes are known to be vapour rich (i.e. 1947 eruption), and the weather radar will also detect the signal from ice and snow particles in the plume (Thorarinsson 1968; Lacasse et al. 2004). There is thus potentiality that the measured and observed plume top is higher than the buoyancy level of pyroclasts in the plume. Scaling parameter Π of 0.2 to 0.26 classifies the 1991 eruption plume as transitional similarly to the climactic Cordón Caulle plume (4–6 June, Bonadonna et al. 2015b) and parts of the May 2010 Eyjafjallajökull plume (Degruyter and Bonadonna 2012).

Conditions of tephra fall

Deposition from the opening phase was to the NNE of Hekla (Fig. 3). The short duration of the explosive activity coupled with a strong wind field probably did not result in a radially spreading umbrella cloud and minimal upwind deposition. A rapid initial drop in mass of tephra deposited along the dispersal axis coincides with deposition of predominantly lapilli during the first 25 km (Figs. 8b, c and 11b), and then more gradual decrease in mass deposition occurred as coarse ash dominates the deposit (>50 wt%). After 65 km, the proportion of fine ash becomes substantial in the deposit (40–20 wt%). This is consistent with size fractionation from a laterally spreading plume and gravitational settling in a turbulent to intermediate regime (Óskarsson 1980; Bursik et al. 1992; Sparks et al. 1992; Bonadonna et al. 1998). Along the dispersal axis, the distance where Md$_\varphi$ and Max$_\varphi$ values level out on Fig. 8b fits roughly with 1 kg m^{-2} isomass line and the 0.2-cm isopach line (60 and 50 km, respectively; Fig. 3) and the last break-in-slope on Fig. 11. Most likely deposition beyond

65 km was characterized by laminar-regime sedimentation (Bonadonna et al. 1998; Bonadonna and Phillips 2003). The deposited material has a mode at 2.5 to 3.5 φ, similar to the finer mode of the TGSD (Fig. 10). There is no significant decrease in grain-size with increasing distance from vent. This is consistent with models where decrease in thinning rate with distance is to be expected when fine ash becomes major part of the deposit (Bonadonna et al. 1998).

The changes in grain-size with transport are considered to reflect the settling velocity and continuous decrease in turbulence and carrying capacity of the plume until around 65 km from went. High sorting (0.9–3 σ$_\varphi$) values during the first 25 km reflect the limited carrying capacity of the plume as most of the mass is deposited within this distance (Figs. 8b and c). Premature sedimentation of ash could have been enhanced by various processes, e.g. induced by snow and as aggregates. Transition to a laminar sedimentation regime and dilution of the plume is marked with no drop in Md$_\varphi$ and Max$_\varphi$.

Total grain-size distribution

Our results show a bimodal TGSD, with a coarse (−3.5 to −2.5 φ) and a fine peak (2.5 to 3.5 φ). The two subpopulations equate to the grain-size modes of samples <10 km from Hekla and 50–120 km from Hekla (Fig. 8a). Bimodal TGSD as reported here is not uncommon. It is a common feature of Hekla eruptions, e.g. from the eruptions in 1104, 1300, 1693, 1766, 1970, and 2000 (Óskarsson 1980; Biass et al. 2014; Janebo 2016). Polymodal TGSD have also been observed in eruptions from other volcanoes, e.g. Mt. St Helens 1980 (Carey and Sigurdsson 1982; Durant et al. 2009), Mt. Spurr 1992 (Durant and Rose 2009), and El Chichón 1982 (Varekamp et al. 1984; Rose and Durant 2009). However, for these non-Icelandic eruptions the polymodal distribution can largely be linked to coeval sedimentation from co-pyroclastic density current (PDC) plumes. For deposits with co-PDC contributions, the fine mode lies at ~5–6 φ (Eychenne et al. 2015), in comparison to 2.5 to 3.5 φ for Hekla 1991. Deposition from a co-PDC plume cannot explain the bimodality for the Hekla 1991 TGSD, as no PDCs were observed during the eruption.

TGSD are very sensitive to the reconstruction method used, but other studies where the TGSD has been computed with same method as here show either unimodal or bimodal TGSDs. Unimodal TGSDs have been reported for, e.g. the Chaitén 2008 eruption (Alfano et al. 2016), the Ruapehu 1996 event (Bonadonna and Houghton 2005), and several subplinian eruptions of Etna (e.g. Scollo et al. 2007; Andronico et al. 2008; Andronico et al. 2009; Andronico et al. 2014) whereas a bimodal distribution is seen for the 2011 eruption of Cordón Caulle (Bonadonna et al. 2015a). In all these eruptions, the TGSD is a result of the primary fragmentation of the magma, and specifically for Cordón Caulle

2011, the shape of the TGSD and significant lack of particles in the 3 φ category was inferred to be a result of complex textural features of the highly vesicular magma (Bonadonna et al. 2015a). The reason for bimodal TGSD is not obvious, but for Hekla 1991 we consider the possibility that the bimodal distribution is a result of the primary fragmentation mechanism of the magma in the shallow conduit. However, the eruptive products of the Hekla 1991 eruption do not show variable texture matching that of the 2011 Cordón Caulle products. Based on the available data, other processes leading to bimodal TGSD cannot be ruled out. Possibilities are e.g. phreatomagmatic activity (which however is unlikely at Hekla), poor sample cover or secondary granulation of lapilli-sized clasts in the conduit, thrust region or the rising plume similarly to what has been proposed to be the source for bimodality of the TGSD from Mt. Spurr 1992 (Durant and Rose 2009).

Although the Voronoi method is designed for non-uniform deposits, the lack of data points between 125 and 195 km from Hekla must be addressed as possible source for TGSD bimodality. Gaps in the dataset might produce TGSDs that are not representative of the associated tephra deposits (Alfano et al. 2016). Lack of the most distal data points however, does not significantly alter the TGSD (Bonadonna et al. 2015a; Alfano et al. 2016). This is due to lower mass contribution and less variability in grain-size distribution of distal samples. The sample gap from 115 to 195 km downwind in the 1991 Hekla dataset (Fig. 8; Supplementary Fig. 1) is in area of low mass accumulation (Fig. 3a) and stable deposited grain-size distribution (Fig. 8b). Therefore, the source of bimodality is not considered to be the spacing of samples. However, this probably results in underestimation of mass contribution of fines in the TGSD (Fig. 10). Thus, the TGSD is considered good approximation and a conservative estimate of mass contributions by ash.

In eruptions where secondary granulation of particles has been proposed as source for bimodal TGSD (i.e. Mt. Spurr 1992) and by co-ignimbrite plumes (i.e. Mt. St Helens 1980), fine ash (<63 μm; >4 φ) is a substantial component of the TGSD (Durant and Rose 2009). In Hekla 1991, fine ash is not a substantial component (Fig. 10).

Therefore, we consider the bimodal TGSD of the Hekla 1991 tephra fall to be a product of the primary fragmentation mechanism(s) taking place in the shallow conduit, and possibly influenced by the pulsating behaviour of the eruption.

Summary and conclusions

The 50-min-long opening subplinian phase of the Hekla 1991 eruption produced a deposit of 8.6×10^9 kg and 0.17 km^3 (0.003 km^3 DRE), with an average mass eruption rate of 2.9×10^6 kg s^{-1} (1100 m^3 s^{-1}). The transitional volcanic plume rose to 11.5 ± 1.2 km in ~10 min. The eruption cloud drifted to the NNE producing a well-defined tephra layer made up of lapilli fall deposits and early-sedimented fines over the first 25 km. There was a gradual decrease in plume turbulence over the first 65 km of transport from vent, as is illustrated by good sorting (from 25 km) and effective size fractionation of tephra. At the 65-km mark, particle sedimentation transitioned to a laminar regime marked with no drop in Md_φ and Max_φ. This coupled with the TGSD indicates that the lapilli-dominated TGSD mode was deposited mostly during the first 25 km of transport. From 25 to 65 km, coarse ash dominates the deposit, whereas the finer TGSD mode coincides with grain-sizes of samples from 65 km onwards. The proximal deposits indicate deposition of tephra from a sustained atmospheric plume with a pulsating source, and snow-enhanced deposition of fines. The calculated TGSD of the deposit is bimodal, and inferred to reflect the primary fragmentation of the magma.

References

Alfano F, Bonadonna C, Watt S, Connor C, Volentic A, Pyle DM (2016) Reconstruction of total grain size distribution of the climactic phase of a long-lasting eruption: the example of the 2008–2013 Caitén eruption. Bull Volcanol 78:46. doi:10.1007/s00445-016-1040-5

Andronico D, Scollo S, Caruso S, Cristaldi A (2008) The 2002-03 Etna explosive activity: tephra dispersal and features of the deposits. Journal of Geophysical Research: Solid Earth 113(4):1–16

Andronico D, Scollo S, Cristaldi A, Ferrari F (2009) Monitoring ash emission episodes at Mt. Etna: the 16 November 2006 case study. J Volcanol Geotherm Res 180:123–134

Andronico D, Scollo S, Lo Castro MD, Cristaldi A, Lodato L, Taddeucci J (2014) Eruption dynamics and tephra dispersal from the 24 November 2006 paroxysm at South-East Crater, Mt Etna, Italy. J Volcanol Geotherm Res 274:78–91

Biass, S., & Bonadonna, C. (2014). TOTGS: Total grainsize distribution of tephra fallout. Retrieved from https://vhub.org/resources/3297

Biass S, Scaini C, Bonadonna C, Folch A, Smith K, Höskuldsson A (2014) A multi-scale risk assessment for tephra fallout and airborne concentration from multiple Icelandic volcanoes—part 1: hazard assessment. Nat Hazards Earth Syst Sci 14:2265–2287

Bonadonna C, Costa A (2012) Estimating the volume of tephra deposits: a new simple strategy. Geology 40(5):415–418

Bonadonna C, Costa A (2013) Plume height, volume, and classification of explosive volcanic eruptions based on the Weibull function. Bull Volcanol 75:1–19

Bonadonna C, Houghton BF (2005) Total grain-size distribution and volume of tephra-fall deposits. Bull Volcanol 67(5):441–456

Bonadonna C, Phillips JC (2003) Sedimentation from strong volcanic plumes. J Geophys Res 108:1–28

Bonadonna C, Ernst GGJ, Sparks RSJ (1998) Thickness variations and volume estimates of tephra fall deposits: the importance of particle Reynolds number. J Volcanol Geotherm Res 81(3–4):173–187

Bonadonna C, Cioni R, Pistolesi M, Elissondo M, Baumann V (2015a) Sedimentation of long-lasting wind-affected volcanic plumes: the example of the 2011 rhyolitic Cordón Caulle eruption, Chile. Bull Volcanol 77:13

Bonadonna C, Pistolesi M, Cioni R, Degruyter W, Elissondo M, Baumann V (2015b) Dynamics of wind-affected volcanic plumes: the example of the 2011 Cordón Caulle eruption, Chile. Journal of Geophysics Research: Solid Earth 120:2242–2261

Bursik MI, Sparks RSJ, Gilbert JS, Carey SN (1992) Sedimentation of tephra by volcanic plumes: I. Theory and its comparison with a study of the Fogo A Plinian deposit, Sao Miguel (Azores). Bull Volcanol 54:329–344

Carey SN, Sigurdsson H (1982) Influence of particle aggregation on deposition of distal tephra from the May 18, 1980, eruption of Mount St. Helens volcano. Journal of Geophysical Research: Solid Earth 87(B8):7061–7072. doi:10.1029/JB087iB08p07061

Carey S, Sparks RSJ (1986) Quantitative models of the fallout and dispersal of tephra from volcanic eruption columns. Bull Volcanol 48:109–125

Carey RJ, Houghton BF, Thordarson T (2009) Tephra dispersal and eruption dynamics of wet and dry phases of the 1875 eruption of Askja Volcano, Iceland. Bull Volcanol 72(3):259–278

Degruyter W, Bonadonna B (2012) Improving on mass flow rate estimates of volcanic eruptions. Geophys Res Lett 39:1–6

Durant AJ, Rose WI (2009) Sedimentological constraints on hydrometeor-enhanced particle deposition: 1992 eruptions of Crater Peak, Alaska. J Volcanol Geotherm Res 186(1–2):40–59

Durant AJ, Rose WI, Carey S, Volentik ACM (2009) Hydrometeor-enhanced tephra sedimentation: constraints from the 18 May 1980 eruption of Mount St. Helens. Journal of Geophysical Research 114:1–21

Eychenne J, Pennec J-L, Troncoso L, Gouhier M, Nedelec J-M (2011) Causes and consequences of bimodal grain-size distribution of tephra fall deposited during the August 2006 Tungurahua eruption (Ecuador). Bull Volcanol 74(1):187–205

Eychenne J, Cashman K, Rust A, Durant A (2015) Impact of the lateral blast on spatial pattern and grain size characteristics of the 18 May 1980 Mount St. Helens fallout deposits. J Geophys Res Solid Earth 120:6018–6038

Fierstein J, Nathenson M (1992) Another look at the calculation of fallout tephra volumes. Bull Volcanol 54(2):156–167

Grönvold K, Larsen G, Einarsson P, Thorarinsson S, Saemundsson K (1983) The Hekla eruption 1980-1981. Bull Volcanol 46:350–363

Gudmundsson A, Sæmundsson K (1992) Heklugosið 1991: Gangur gossins og aflfræði Heklu. Náttúrufræðingurinn 61:145–158

Gudmundsson A, Oskarsson N, Grönvold K, Saemundsson K, Sigurdsson O, Stefansson R, Thordarson T (1992) The 1991 eruption of Hekla, Iceland. Bull Volcanol 54(3):238–246

Gurioli L, Houghton BF, Cashman KV, Cioni R (2005) Complex changes in eruption dynamics during the 79 AD eruption of Vesuvius. Bull Volcanol 67(2):144–159. doi:10.1007/s00445-004-0368-4

Haraldsson KÖ (2001) The Hekla 2000 eruption, distribution of ash from the first days of the eruption (in Icelandic). BSc thesis. University of Iceland, Reykjavík

Höskuldsson Á, Óskarsson N, Pedersen R, Grönvold K, Vogfjörð K, Ólafsdóttir R (2007) The millennium eruption of Hekla in February 2000. Bull Volcanol 70(2):169–182

Houghton BF, Wilson CJN (1989) A vesicularity index for pyroclastic deposits. Bull Volcanol 51:451–462

Houghton BF, Wilson CJN, Del Carlo P, Coltelli M, Sable JE, Carey R (2004) The influence of conduit processes on changes in style of basaltic Plinian eruptions: Tarawera 1886 and Etna 122 BC. J Volcanol Geotherm Res 137:1–14

Inman D (1952) Measures for describing the size distribution of sediments. J Sediment Petrol 22(3):125–145

Jakobsson S (1979) Petrology of recent basalts of the Eastern Volcanic Zone, Iceland. Acta Naturalia Islandica 26:1–103

Janebo MH (2016) Historical explosive eruptions in Hekla and Askja volcanoes; eruption dynamics and source parameters. PhD dissertation. University of Hawaii at Manoa, Honolulu

Janebo MH, Thordarson T, Houghton BF, Larsen G, Carey RJ (2016) Dispersal of key subplinian-Plinian tephra from Hekla volcano, Iceland: implications for eruption source parameters. Bull Volcanol 78. doi:10.1007/s00445-016-1059-7

Jóhannesson H, Einarsson S (1990) Glefsur úr sögu hrauna og jarðvegs sunnan Heklu. In: Arnalds A (ed) Græðum Ísland. Landgræðslan, Reykjavik, pp 123–136

Jóhannesson H, Sæmundsson K (1998) Geological map of Iceland, 1: 500.000 bedrock geology, Reykjavik. Náttúrufræðistofnun Íslands, Reykjavík

Kaminski E, Jaupart C (1998) The size distribution of pyroclasts and the fragmentation sequence in explosive volcanic eruptions. J Geophys Res 103(98):29759–29779

Klug C, Cashman KV (1996) Permeability development in vesiculating magmas: implications for fragmentation. Bull Volcanol 58:87–100

Kueppers, U., Scheu, B., Spieler, O., & Dingwell, D. B. (2006). Fragmentation efficiency of explosive volcanic eruptions: a study of experimentally generated pyroclasts, 153, 125–135

Lacasse C, Karlsdóttir S, Larsen G, Soosalu H, Rose WI, Ernst GGJ (2004) Weather radar observations of the Hekla 2000 eruption cloud, Iceland. Bull Volcanol 66:457–473

Larsen G, Thorarinsson S (1977) H4 and other acid Hekla tephra layers. Jökull 27:28–46

Larsen G, Vilmundardóttir EG, Thorkelsson B (1992) Heklugosið 1991 : Gjóskufallið og gjóskulagið frá fyrsta degi gossins. Náttúrufræðingurinn 61:159–176

Lautze NC, Houghton BF (2006) Linking variable explosion style and magma textures during 2002 at Stromboli Volcano, Italy. Bull Volcanol 69(4):445–460

Linde AT, Agustsson K, Sacks IS, Stefansson R (1993) Mechanism of the 1991 eruption of Hekla from continuous borehole strain monitoring. Nature 365(21):737–740

Mastin LG, Guffanti M, Servranckx R, Webley P, Barsotti S, Dean K, Waythomas CF (2009) A multidisciplinary effort to assign realistic source parameters to models of volcanic ash-cloud transport and dispersion during eruptions. J Volcanol Geotherm Res 186(1–2):10–21

Newhall CG, Self S (1982) The volcanic explosivity index (VEI) an estimate of explosive magnitude for historical volcanism. J Geophys Res 87(C2):1231

Oddsson B, Gudmundsson MT, Larsen G, Karlsdóttir S (2012) Monitoring of the plume from the basaltic phreatomagmatic 2004 Grímsvötn eruption—application of weather radar and comparison with plume models. Bull Volcanol 74:1395–1407

Óskarsson N (1980) The interaction between volcanic gases and tephra: fluorine adhering to tephra of the 1970 Hekla eruption. J Volcanol Geotherm Res 8:251–266

Polacci M, Baker DR, Mancini L, Polacci M, Baker DR, Mancini L, Tromba G (2006) Three dimensional investigation of volcanic textures by X-ray microtomography and implications for conduit processes. Geophys Res Lett 33:1–5

Pyle DM (1989) The thickness, volume and grainsize of tephra fall deposits. Bull Volcanol 51:1–15

Rose WI, Durant AJ (2009) El Chichón volcano, April 4, 1982: volcanic cloud history and fine ash fallout. Nat Hazards 51(2):363–374

Sæmundsson K (1979) Outline of the geology of Iceland. Jökull 29:7–28

Scollo S, Del Carlo P, Coltelli M (2007) Tephra fallout of 2001 Etna flank eruption: analysis of the deposit and plume dispersion. J Volcanol Geotherm Res 160(1–2):147–164

Soosalu H, Einarsson P, Jakobsdottir S (2003) Volcanic tremor related to the 1991 eruption of the Hekla Volcano, Iceland. Bull Volcanol 65(8):562–577

Sparks RSJ, Bursik MI, Ablay GJ, Thomas RME, Carey SN (1992) Sedimentation of tephra by volcanic plumes. Part 2: controls on thickness and grain-size variations of tephra deposits. Bull Volcanol 54:685–695

Sparks RSJ, Bursik MI, Carey SN, Gilbert JS, Glaze LS, Sigurdsson H, Woods AW (1997) Volcanic plumes, 1st edn. Wiley, Chichester

Stevenson, J., Larsen, G., & Thordarson, T. (2015). Physical volcanology of the prehistoric Hekla 3 and Hekla 4 eruptions, Iceland. *EGU General Assembly, abstract id.4207*

Thorarinsson S (1968) Heklueldar. Rangæingafélagið, Reykjavik

Thorarinsson S, Sigvaldason GE (1972) The Hekla eruption of 1970. Bull Volcanol 36(2):269–288

Thordarson T, Larsen G (2007) Volcanism in Iceland in historical time: volcano types, eruption styles and eruptive history. J Geodyn 43(1): 118–152

Þráinsson, B. Þ. (1991). *Iceland national radio, 19:00 news*, January 17th 1991

Varekamp JC, Luhr JF, Prestegaard KL (1984) The 1982 eruptions of El Chichón Volcano (Chiapas, Mexico): character of the eruptions, ash-fall deposits, and gas phase. J Volcanol Geotherm Res 23(1–2):39–68

Walker GPL (1973) Explosive volcanic eruptions—a new classification scheme. Geol Rundsch 62(2):431–556